Investigation of the flow characteristics of a falling film along an inclined surface with planar laser-induced fluorescence method

X. Chen[a], C. Wang[a], Y. Song[a], X.L. Ouyang[a], P.X. Jiang[a,*], S.Q. Shen[b]

[a]*Department of Thermal Engineering, Tsinghua University, Beijing, China, Tel. +86 10 62772661;*
emails: jiangpx@mail.tsinghua.edu.cn (P.X. Jiang), rnxchenxue@mail.tsinghua.edu.cn (X. Chen),
cwang0302@163.com (C. Wang), ysong@tsinghua.edu.cn (Y. Song), ouyangxl@mail.tsinghua.edu.cn (X.L. Ouyang)
[b]*School of Energy and Power Engineering, Dalian University of Technology, Dalian, Liaoning, China, email: zzbshen@dlut.edu.cn*

ABSTRACT

Planar laser-induced fluorescence technology was used to investigate the three-dimensional film thickness distribution of falling film on an inclined surface. The film thickness distributions in both the streamwise and the spanwise direction were presented for various inclination angles, the surface tensions and the flow rates. The results show that the spanwise liquid film distribution has a "bow" shape, the film thickness and film width increase with increasing flow rate. The film width decreases with increasing liquid surface tension, but the film thickness of the ripples increases.

Keywords: Falling film; Film thickness; Flow state; Planar laser-induced fluorescence

1. Introduction

Falling film evaporation is widely utilized in nuclear industry [1], desalination [2], sewage treatment, chemical engineering [3], food processing [4] and other fields due to their highly efficient heat transfer. The flow state of the liquid film on the surface dominates the heat and mass transfer and greatly influences the system efficiency. Previous study [2] shows that the film thickness significantly affects the falling film evaporation efficiency with a thicker liquid film increasing the thermal resistance which reduces heat transfer coefficient. Hence, numerous studies have investigated the flow characteristics of liquid falling films on solid surfaces.

Moran et al. [5] measured the film thickness on a long channel (a copper bottom plate and polycarbonate sidewalls) with an 80 mm × 1,920 mm plate at 45° inclination angle by using photochromatic dye that could be exposed by UV light. Their result indicated that the film thickness was slightly underpredicted by Nusselt's theory at Re = 11–220. Roy and Jain [6] measured the falling film thickness on a

190 mm × 318 mm Plexiglas plate with side walls. Two points on the centerline 76 and 216 mm from the distributor flow outlet were detected by using two capacitance probes for various inclination angles and Reynolds numbers. Takamasa and Hazuku [7] studied liquid falling film thickness fluctuations on a 460 mm × 210 mm sidewall-confined vertical plate by using laser focus displacement measurements with their results agreeing well with Nusselt's theoretical equation and the film thickness being independent of the entry length at low Reynolds numbers. Zhou et al. [8] investigated the flow in a falling film on a confined inclined 622 mm × 155 mm stainless steel plate. They used the confocal chromatic point measurement to detect the film thickness with different distributor designs, inclination angles and Reynolds numbers. Their results showed that the film thickness decreases with the inclined angle and increases with the Reynolds number. Charogiannis et al. [9–11] experimentally investigated the film thickness and its fluctuations of a confined flow on an inclined surface with sidewalls. The centerline film thickness along streamwise direction was measured using the laser-induced fluorescence method.

Besides falling films on plates with confined sidewalls, studies have also emphasized on unconfined falling films.

* Corresponding author.

Johnson et al. [12] used a fluorescent imaging method to study the rivulet flow patterns on an inclined plate and measured the rivulet thickness from calibrated outgoing light intensities. They found that the rivulet widths narrowed with increasing the inclination angles. Zhang et al. [13] examined the spread area of a falling film along unconfined vertical heated and cooled surface using an infrared camera to show that the film width increases on the cooled surface and decreases on the heated surface. Lan et al. [14] observed the liquid film flow on an unconfined inclined plate with the non-sequential film thickness distribution on a cross-section in the streamwise direction detected by a laser focus displacement instrument. They found that the film thickness decreases with increasing inclination angle and increases with the flow rate. They also pointed out that the ripples form on the two sides of the liquid film along the spanwise direction and that the ripple thickness increases with the surface tension. However, the ripple region interface could not be clearly detected for small surface tension. Lan et al. [14,15] also used the volume of fluid method to simulate the three-dimensional film flow and indicated that the surface tension and contact angle affect the film width obviously, but the centerline thickness of the liquid film is almost independent of the surface tension and contact angle.

Various measurement methods have been developed to detect the gas–liquid interface for the liquid film. The conductivity method [16] is convenient and has been widely used despite the relatively large error. The capacitance method [17] has been developed to avoid contact measurement, but it has not been widely used due to the restricted usage conditions. Optical methods, such as the laser confocal method [18], confocal chromatic method [8] and laser-induced fluorescence method [9,19], have been developed rapidly in recent years to give fast and accurate measurement.

Most previous studies have focused on falling films along plates with sidewalls, with limited studies of unconfined falling films. Also, most methods for detecting the interface have been the point measurements. Hence, planar laser-induced fluorescence (PLIF) was used here to measure the continuous three-dimensional thickness distributions of falling films on inclined plates, in order to investigate the effects of Reynolds number, surface tension and inclination angle on the film thickness.

2. Apparatus and methods

The experimental apparatus included a fluid circulation system and an optical imaging system as shown in Fig. 1. In the fluid circle system, the experimental fluid was pumped from the lower tank into the upper tank and then passed through a valve and a flowmeter before entering the distributor. A falling film then formed on the inclined plate. The fluid passed through the optical measurement zone, into the reservoir, and then was pumped back to the storage tank. The distributor was designed as a box with a wedge-shaped outlet fixed perpendicularly above the plate. The outlet was 2 mm wide and 60 mm long, and placed 2 mm above the plate to produce a uniform liquid film. Rhodamine B solutions and Rhodamine B–surfactant solutions were used as the experimental fluids and the surface tensions were listed in Table 1 (Rhodamine B, CAS81-88-9, Tokyo Chemical Industry Co., Ltd. (Tokyo, Japan); surfactant,
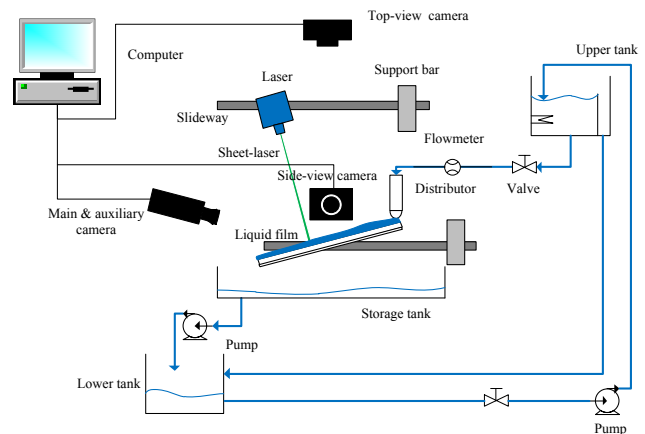

Fig. 1. Experimental system.

Table 1
Surface tension of the test fluid

Test fluid	Composition	Surface tension, N/m
Sample #1	Water + Rhodamine B	0.066
Sample #2	Water + Rhodamine B + Surfynol-465	0.050

Surfynol-465, Air Products and Chemicals, Inc., Allentown, PA, USA). The addition of Surfynol-465 is 0.75% (wt%). The surface tension was measured by Wilhelmy plate method (Krüss Tensiometer K100). The silica glass base plate was 120 mm wide and 200 mm long.

In optical imaging system, the PLIF method was used to measure the three-dimensioned thickness distribution as shown in Fig. 2. The optical equipment and the test plate with the adjustable support were all fixed on the optical platform with the movement regulated by micrometers. The PLIF system included as follows:

- Laser source with a sheet optical lens: A continuous solid-state laser (Solo XT 532 nm, New Wave Research, Inc., Fremont, CA, USA) with λ = 532 nm (green laser) was used in this experiment. The laser sheet was 0.2 mm wide and 120 mm long, respectively, and the laser source was located 500 mm away from the test plate.
- Cameras: The test scope for investigating the film thickness along spanwise direction in this experiment was relatively large, so a high resolution camera was needed to guarantee the accuracy. A high definition digital camera, a Canon 7D with a Canon EF 100 mm Marco lens, was used in this experiment as the main camera. Images with 5,184 × 3,456 pixels were obtained at 0.5 fps with exposure time of 1/1,000 s. An electronic front-curtain shutter and a second-curtain with a time-lag release were used in the shooting to eliminate the influence of vibration. With the adjustable support, the viewing angles could be adjusted at the desired angles to avoid the potential influence of film fluctuations. A high speed camera, Basler CCD camera at 1,000 fps with 1,280 × 512 pixels, was used to detect the variations of local film thickness as
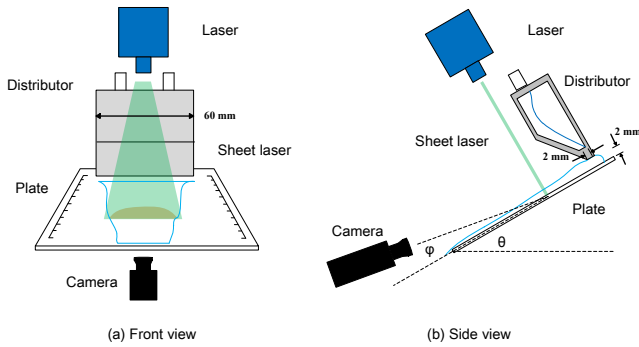
Fig. 2. Schematic of the planar laser-induced fluorescence system.

an auxiliary camera. A Nikkor AF 50 mm lens and several extension rings were used to achieve a reasonable view size. A side view camera and a top view camera were also used to confirm the equipment positions and the angle in real time.

- Band filter: A band filter was installed in front of the camera lens to block light with $\lambda < 550$ nm. Thus, the camera can detect the fluorescent but not the light scattered from the gas–liquid interface to improve the accuracy.
- Fluorescent dye: Rhodamine B is a common dye that strongly fluoresces with the maximum wavelength of about 580 nm when excited by a laser at $\lambda = 532$ nm [20]. The concentration of the Rhodamine B aqueous solution was 0.1 g/L, which had little effect on the physical properties [21,22].

3. Experimental procedure and data processing

The test plate, laser and camera were adjusted as shown in Fig. 2 for the desired inclination angle. The sheet laser was aligned perpendicularly to surface at the desired 0.2 mm line wide scale marks engraved on both edges of the plate. A calibration board was then placed perpendicularly to the surface at the desired scale marks to focus and calibrate the camera. The flow rate was then adjusted to the desired value and the fluorescent agent in the liquid was induced by the sheet laser. After the falling film became stable, repeated test images of the gas–liquid interface were captured. Fig. 3 shows a visualized falling film in experiment.

The image processing procedure is shown in Fig. 4. An in-house MATLAB-based processing program was used to identify the gas–liquid interface. The original images were transformed into a two-dimensional matrix. Fig. 4(a) shows an original image of the gas–liquid interface from the laser-induced fluorescence; Fig. 4(b) shows the 8-bit gray-scale image of Figs. 4(a) and (c) shows the matrix of the 8-bit gray-scale values. The liquid–gas interface, which is the liquid film profile, was obtained from the test images using the maximum gradient method [9] with a row array shown in Fig. 4(d). Any point far from the interface was assumed to be signal noise, and replaced by the value which was linearly interpolated from the two adjacent points. The physical length per pixel was calculated from calibration broad with the centerline coordinate of the desired marks used as the baseline coordinate. Hence, the relative film thickness was obtained by multiplying the physical length per pixel by the
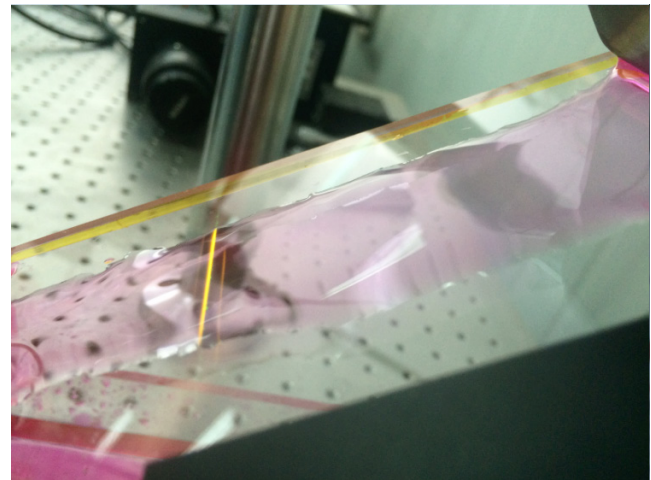

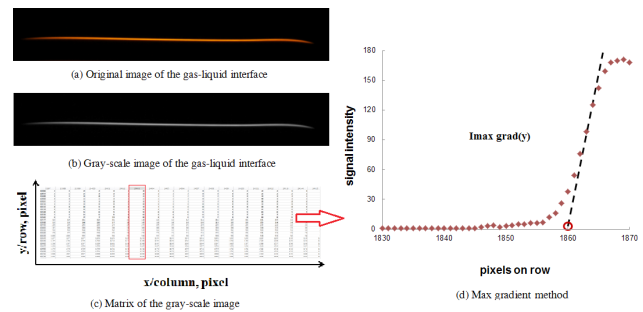Fig. 3. Visualized film flow.

Fig. 4. Image processing procedure.

pixel number of the film thickness which was the difference between the coordinate value of the gas–liquid interface and that of the baseline. Finally, the absolute film thickness was calculated after correcting the relative film thickness for the view angle. All the measurements were taken with the flow rate being increased at each step.

The PLIF method accuracy was compared with chromatic confocal displacement sensor (CCDS; ACR-HNDS100) measurement in initial tests. The compared tests were performed for sample #2 with $l = 50$ mm, $q = 2.78$ g/s and $\theta = 20°$. A mean film thickness of 0.351 mm ± 0.030 mm for PLIF method and 0.340 mm ± 0.019 mm for CCDS system were measured during a test time. These tests show a good agreement between the two methods. In this study, the PLIF method can achieve line measurement, but it is limited by the fluorescence intensity and the gray-scale recognition of camera, therefore, when the film thickness is less than about 0.08 mm, it will be difficult to detect the interface.

The experimental system error included the errors in the angle measurement, flowmeter and image recognition process. The angle error was 0.083° and the flowmeter error was 1.5%. Due to the geometrical relationship, the angle error can be neglected in this experiment. The image recognition error was due to the boundary detection when the coordinate value at a noisy point was replaced by the average of the two adjacent points (a "jump" in the gas/liquid interface along

the x-coordinate was classified as a noisy point if the variation was greater than 1 pixel). The boundary identification error was not more than 2% of the average film thickness in the center region based on the minimum number of pixels for the film thickness measurement. The spatial resolution varies slightly due to the change of target focus plane. For example, in this study, the physical length per pixel is 0.0096 mm at $l = 50$ mm for the high definition digital camera. The values of the liquid film thicknesses were time-averaged values unless otherwise stated.

4. Results and discussion

4.1. Flow state

The relationship between the film Reynolds number and flow rate can be defined as $Re = \Gamma/\mu$, μ refers to the dynamic viscosity and $\Gamma = q/l_e$ refers to spray density, q and l_e are the flow rate and effective spray length, respectively. The centerline film thickness for sample #2 at 50 mm from the inlet with the flow rate $q = 2.78$ g/s and $\theta = 20°$ is shown in Fig. 5. The film thickness variation with time was detected by the high speed CCD camera at 1,000 fps. The film thickness varies randomly with time, but the whole fluctuation maintains in a certain range.

The scatters of gas–liquid interface (namely the film thickness) for five images taken 50 mm from the inlet at $q = 2.78$ g/s and $\theta = 20°$ are shown in Fig. 6. The liquid film profile along the spanwise direction has a "bow" distribution and can be divided into the "ripple region" with large film thicknesses on both sides and the "center region" at middle. In the ripple region, the film thickness increases sharply from the three-phase contact line and then decreases slightly after reaching a maximum value. In the center region, the film thickness is relatively stable, but it also shows a slight rising trend from side to center.
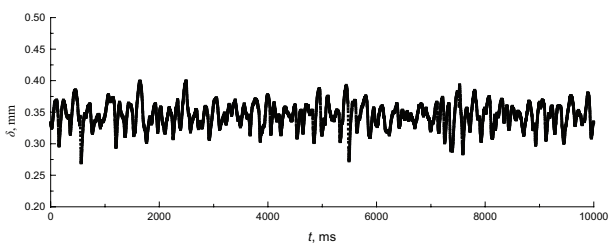
A three-dimensional image of the flow in the falling film along the inclined surface is shown in Fig. 7 for $q = 2.78$ g/s and $\theta = 20°$. This figure was obtained by combining multiple images of spanwise sections. It shows that the spanwise width and the section area of the falling film decrease along the streamwise direction, because the cohesive force is larger than the adhesive force, the surface tension reduces the surface area of liquid film. The film is 46.13 mm wide at $l = 50$ mm while it is 40.75 mm at $l = 85$ mm. In addition, the liquid film shrinkage mainly occurs in center region of the film.

The shape and height of the falling film in the ripple region are almost constant along the streamwise direction, while the film thickness in the center region increases slightly in the streamwise direction. The thickness in the middle of the center region increased about 5.3% from $l = 50$ to 85 mm. The flow state shows a good reproducibility, but sometimes it is affected by the hysteresis. That is why all the measurements were taken with the flow rate being increased at each step.

4.2. Effect of flow rate on the film thickness

Figs. 8(a) and (b) present the film thickness variations of sample #1 for various flow rates with $l = 50$ mm and $\theta = 20°$. In general, the film thickness increases with the flow rate, which is agreed with Lan et al. [14]. It should be noted that the increase is not continuous, but in stages. When the interval of the flow rate increase is small, the film becomes thicker but the width remains consistent, as shown in Fig. 8(a). When the enhancement in flow rate exceeds a critical value, the film width extends suddenly and then begins to thicken again till the next extend, as shown in Fig. 8(b). This shows a phenomenon which is similar to dynamic contact angle hysteresis of a droplet.

4.3. Effect of surface tension on the film thickness

Fig. 9 shows the comparison of the film thickness distributions between samples #1 and #2 for $q = 2.78$ g/s, $\theta = 40°$ and $l = 50$ mm. The film thickness of sample #1 with the higher surface tension in the ripple region is about 0.10 mm larger than that of sample #2. The influence of the surface tension on the film thickness in the center region is less than in the ripple

Fig. 5. Film thickness variation with time for sample #2 with $l = 50$ mm, $q = 2.78$ g/s and $\theta = 20°$.

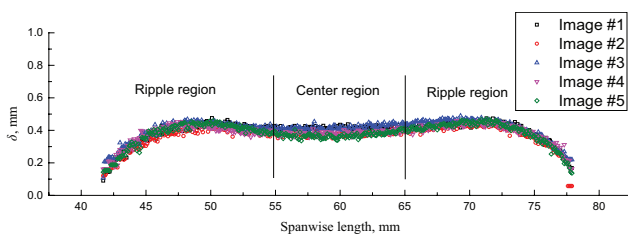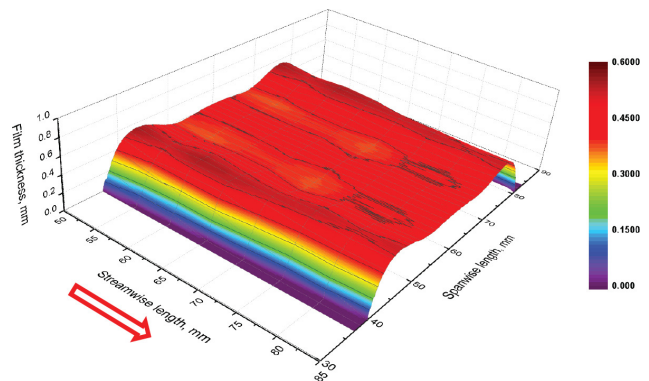Fig. 6. Film thickness distribution along the spanwise direction for sample #1 with $q = 2.78$ g/s and $\theta = 20°$.

Fig. 7. Film flow along the streamwise for sample #1 with $q = 2.78$ g/s and $\theta = 20°$.

Fig. 10. Effect of inclination angle on film thickness for sample #2 with $l = 50$ mm.
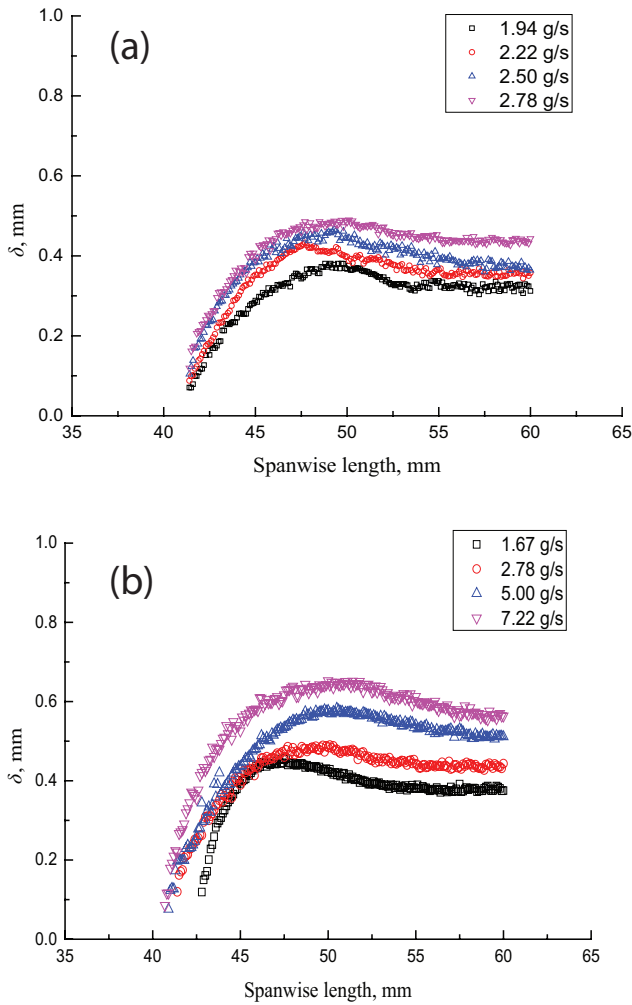

Fig. 8. Film thickness variation with the flow rate for sample #1 with $l = 50$ mm and $\theta = 20°$.
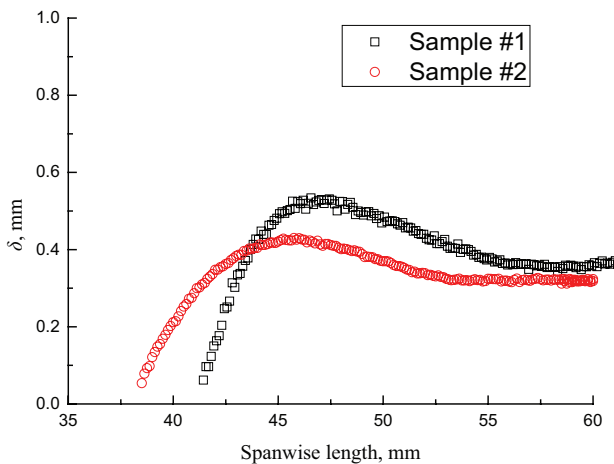
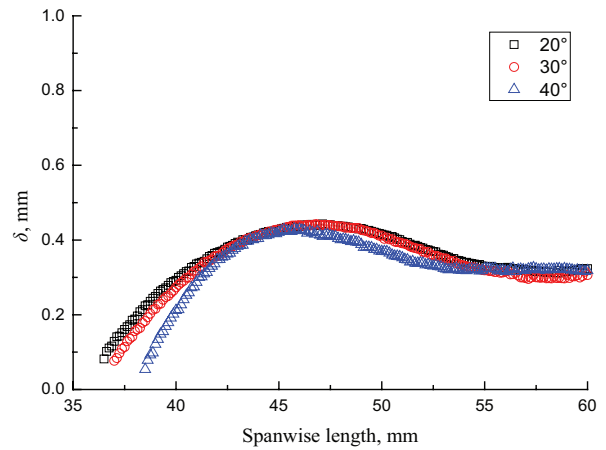Fig. 9. Effect of surface tension on film thickness with $q = 2.78$ g/s, $\theta = 40°$ and $l = 50$ mm.

region with sample #1 in the center region only 0.04 mm higher. The falling film width of sample #1 with the higher surface tension is less than that of sample #2 with sample #2 being 17.8% wider than sample #1 in Fig. 9. The larger surface tension causes the film width to shrink much faster, because the larger surface tension produces a larger cohesive force and a lower adhesive force.

4.4. Effect of inclination angle on the film thickness

The effect of the inclination angle on the film profile for sample #2 at $l = 50$ mm is presented in Fig. 10. The inclination angle influences the gravitation force on the falling film with a larger inclination angle giving a higher gravitational force, which results in a higher film velocity, a slightly thinner film thickness and a smaller film width.

5. Conclusions

The laser-induced fluorescence method was used to measure the three-dimensional film thickness profile of a falling film along an inclined plate without confined sides. The effects of flow rate, surface tension and inclination angle on film thickness were analyzed with the following conclusions:

- The film thickness across the spanwise direction has a bowed shape with ripple regions on the two sides and center region between them.
- The film width decreases with the increase of the streamwise length; the center region width decreases with the increase of the streamwise length while the center region height increases slightly.
- With the flow rate increases, the film thickness and the film width both increase.
- The maximum film thickness at the ripple region increases with the increasing surface tension; the liquid film width decreases as the surface tension increases.
- The film thickness and film width both decrease as the inclination angle increases.

Symbols

Re — Reynolds number
g — Gravitational constant, m/s^2
h — Film thickness, mm
l — Streamwise length, mm
l_e — Effective spray length, mm
Γ — Spray density, kg/(m s)
μ — Dynamic viscosity, Pa s
β — Contact angle, °
λ — Wave length, nm
θ — Inclined angle, °
ϕ — Viewing angle, °
δ — Film thickness, mm

References

[1] Y.Q. Yu, S.J. Wei, Y.H. Yang, X. Cheng, Experimental study of water film falling and spreading on a large vertical plate, Prog. Nucl. Energy, 54 (2012) 22–28.

[2] S.Q. Shen, X. Chen, X.S. Mu, Y.X. Wang, L.Y. Gong, Heat transfer characteristics of horizontal tube falling film evaporation for desalination, Desal. Wat. Treat., 55 (2015) 3343–3349.

[3] I. Yoshiyuki, X. Chen, Flow transition behavior of the wetting flow between the film flow and rivulet flow on an inclined wall, J. Fluids Eng., 133 (2011) 1–6.

[4] E. Fuchs, A. Boye, R. Murcek, J.P. Majschak, An experimental comparison of film flow parameters and cleaning behaviour of falling liquid films for different tilt angles, Food Bioprod. Process., 93 (2015) 318–326.

[5] K. Moran, J. Inumaru, M. Kawaji, Instantaneous hydrodynamics of a laminar wavy liquid film, Int. J. Multiphase Flow, 28 (2002) 731–755.

[6] R.P. Roy, S. Jain, A study of thin water film flow down an inclined plate without and with countercurrent air flow, Exp. Fluids, 7 (1989) 318–328.

[7] T. Takamasa, T. Hazuku, Measuring interfacial waves on film flowing down a vertical plate wall in the entry region using laser focus displacement meters, Int. J. Heat Mass Transfer, 43 (2000) 2807–2819.

[8] D.W. Zhou, T. Gambaryan-Roisman, P. Stephan, Measurement of water falling film thickness to flat plate using confocal chromatic sensing technique, Exp. Therm. Fluid Sci., 33 (2009) 273–283.

[9] A. Charogiannis, J.S. An, C.N. Markides, A simultaneous planar laser-induced fluorescence, particle image velocimetry and particle tracking velocimetry technique for the investigation of thin liquid-film flows, Exp. Therm. Fluid Sci., 68 (2015) 516–536.

[10] A. Charogiannis, F. Denner, B.V. Wachem, S. Kalliadasis, C.N. Markides, Detailed hydrodynamic characterization of harmonically excited falling-film flows: a combined experimental and computational study, Phys. Rev. Fluids, 2 (2017) 014002-1-37.

[11] C.N. Markides, R. Mathie, A. Charogiannis, An experimental characterization of spatiotemporally resolved heat transfer in thin liquid-film flows falling over an inclined heated foil, Int. J. Heat Mass Transfer, 93 (2015) 872–888.

[12] M.G. Johnson, R.A. Schluter, M.J. Miksis, S.G. Bankoff, Experimental study of rivulet formation on an inclined plate by fluorescent imaging, J. Fluid Mech., 394 (1999) 339–354.

[13] F. Zhang, Y.T. Wu, J. Geng, Z.B. Zhang, An investigation of falling liquid films on a vertical heated/cooled plate, Int. J. Multiphase Flow, 34 (2008) 13–28.

[14] H. Lan, J.L. Wegener, B.F. Armaly, J.A. Drallmeier, Developing laminar gravity-driven thin liquid film flow down an inclined plane, J. Fluids Eng., 132 (2010) 081301.

[15] H. Lan, M. Friedrich, B.F. Armaly, J.A. Drallmeier, Simulation and measurement of 3D shear-driven thin liquid film flow in a duct, Int. J. Heat Fluid Flow, 29 (2008) 449–459.

[16] H. Hou, Q.C. Bi, H. Ma, G. Wu, Distribution characteristics of falling film thickness around a horizontal tube, Desalination, 285 (2012) 393–398.

[17] L. Xu, S.C. Wang, Y.X. Wang, Y. Ling, Flowing state in liquid films over horizontal tubes, Desalination, 156 (2003) 101–107.

[18] J.L. Wegener, J.A. Drallmeier, Measurement of Thin Liquid Film Characteristics Using Laser Focus Displacement Instruments for Atomization Applications, 2th Annual Conference on Liquid Atomization and Spray Systems, Cincinnati, USA, 2010.

[19] X. Chen, S.Q. Shen, Y.X. Wang, J.X. Chen, J.S. Zhang, Measurement on thickness distribution of falling film around horizontal tube with laser-induced fluorescence technology, Int. J. Heat Mass Transfer, 89 (2015) 707–713.

[20] I.L. Arbeloa, K.K. Rohatgi-mukherjee, Solvent effect on photophysics of the molecular forms of rhodamine B. Solvation models and spectroscopic parameters, Chem. Phys. Lett., 128 (1986) 474–479.

[21] D. Gstoehl, J.F. Roques, P. Crisinel, J.R. Thome, Measurement of falling film thickness around a horizontal tube using a laser measurement technique, Heat Transfer Eng., 25 (2004) 28–34.

[22] X. Wang, M. He, H. Fan, Y. Zhang, Measurement of Falling Film Thickness Around a Horizontal Tube Using Laser-Induced Fluorescence Technique, The Sixth International Symposium on Measurement Techniques for Multiphase Flows, Okinawa, Japan, 2009.
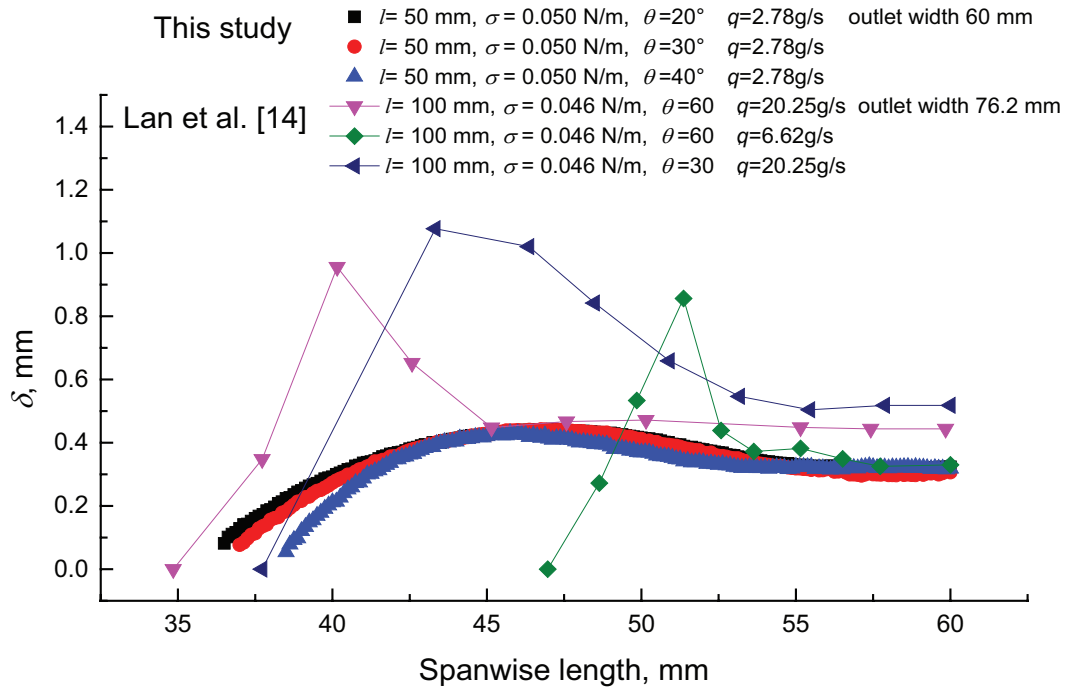
Supplementary information

Fig. S1. The comparison with Lan et al. [14].